atmosphere

MDPI

Article

Numerical Simulations of the Impacts of Mountain on Oasis Effects in Arid Central Asia

Miao Zhang [1,2,3,4], Geping Luo [1,*], Rafiq Hamdi [5,6], Yuan Qiu [1,3], Xinxin Wang [1,3], Philippe De Maeyer [2,4] and Alishir Kurban [1,4]

1 State Key Laboratory of Desert and Oasis Ecology, Xinjiang Institute of Ecology and Geography, Chinese Academy of Sciences, No. 818 South Beijing Road, Urumqi 830011, China; miaomiaozpb@163.com (M.Z.); qiuyuan.cas@gmail.com (Y.Q.); wangxinxin0803@gmail.com (X.W.); alishir@ms.xjb.ac.cn (A.K.)
2 Department of Geography, Ghent University, Krijgslaan 281, S8, B-9000 Ghent, Belgium; philippe.demaeyer@ugent.be
3 University of the Chinese Academy of Sciences, Beijing 100049, China
4 Sino-Belgian Joint Laboratory for Geo-information, Xinjiang Institute of Ecology and Geography and Ghent University, Urumqi 830011, China and B-9000 Ghent, Belgium
5 Royal Meteorological Institute, Avenue Circulaire, 3, B-1180 Brussels, Belgium; rafiq.hamdi@meteo.be
6 Department of Physics and Astronomy, Ghent University, B-9000 Ghent, Belgium
* Correspondence: luogp@ms.xjb.ac.cn; Tel.: +86-991-7823127; Fax: +86-991-7885320

Introduction

Table S1 shows land cover type and code of the 2012LC. Table S2 shows land use type and its categories in WRF and the 2012LC. This table can be complement for explaining classification system of the 2012LC and how the land use values of the 2012LC is converted into WRF land use values.

Text S1 to S4 show the high-resolution LC and real-time albedo, LAI and GVF in detail, which were used to replace corresponding basis datasets in WRF model.

Figure S1 shows Mean 2-m air temperatures (T2) from the non-mountain simulation, and differences between mod and non-mountain simulations during daytime and nighttime.

Figure S2. As Figure S1, but for specific humility.

Figure S3. The W component difference between the mod simulation and non-oasis simulation during daytime and nighttime.

Figure S4. The mean sensible heat flux from the (a, b) mod simulation nd (c,d) non-mountain simulation during daytime and nighttime, and (e, f) differences between mod and non-oasis simulations and (g, h) differences between mod and non-mountain simulations. The black dotted line represents the oasis border.

Figure S5. As Figure S4, but for latent heat flux.

S1. LU

The default Land Cover types (LC) data included in the WRF are originally from the U.S. Geological Survey (USGS) derived from the Advanced Very High Resolution Radiometer (AVHRR) for April 1992-March 1993, which classifies LC into 24 categories (Table S2) [*Wen, Lu et al.*, 2012]. A high-resolution LU image was produced for 2012 (2012LC) using visual interpretations based on Landsat images and a 1:1,000,000 topographic map. This image was generated by the Xinjiang Institute of Ecology and Geography (XIEG), Chinese Academy of Sciences (CAS) [*Chen*, 2008]. The 2012LC has a spatial resolution of 30 m and adopts a hierarchical classification system, including 6 categories and 25 subcategories (Table S1). We converted it into the USGS classification system according to the corresponding relationships shown in Table S2, and upscaled the LU to 1 km using a majority resampling technique. There were 9 land use types in the study area (shown in italic Table S2).

Table S1. Classification system of the 2012LC.

Land cover categories code	Land cover categories	Subcategories code	Subcategories
1	Cropland	11	Irrigated crops (rice, lotus and other aquatic crops)
		12	Non-irrigated crops (rainfed croplands)
2	Forestland	21	Closed(>30%)natural and artificial forests
		22	Closed(>40%) Shrub
		23	Closed(10% ~ 30%) woodland
		24	Other woodland (orchards, mulberry)
3	Grassland	31	closed (>50%) grassland
		32	Closed- to-open 20% ~ 50% grassland
		33	Open 5% ~ 20% grassland
4	Water and Wetland	41	Rivers and canals
		42	Lakes
		43	Reservoir ponds
		44	Snow and ice
		45	Intertidal
		46	Floodplain
5	Settlements	51	Cities and towns
		51	Villages
		53	Other construction lands
6	Others	61	Sandy land
		62	Gobi
		63	Saline
		64	Marsh
		65	Bare
		66	Bare rock
		67	Others

Table S2. Land use type and its categories in WRF and the 2012LC.

Land Cover Type	WRF	2012LC
Urban and Built-Up Land	1	51
Dryland Cropland and Pasture	2	
Irrigated Cropland and Pasture	3	11, 12, 52, 21 (if DEM < 1,500)
Mixed Dryland/Irrigated Cropland and Pasture	4	
Cropland/Grassland Mosaic	5	
Cropland/Woodland Mosaic	6	
Grassland	7	31 (if DEM ≥ 1,000), 32 (if DEM ≥ 1,000), 33 (if DEM ≥ 1,000)
Shrubland	8	23, 22 (if DEM < 1,500)
Mixed Shrubland/Grassland	9	
Savanna	10	
Deciduous Broadleaf Forest	11	
Deciduous Needleleaf Forest	12	
Evergreen Broadleaf Forest	13	
Evergreen Needleleaf Forest	14	21 (if DEM ≥ 1,500), 22 (if DEM ≥ 1,500)
Mixed Forest	15	
Water Bodies	16	41, 42, 43, 46,

Herbaceous Wetland	17	
Wooded Wetland	18	
Barren or Sparsely Vegetated	19	61, 62, 63, 65, 67, 66 (if DEM < 3,400), 31 (if DEM < 1,000), 32 (if DEM < 1,000), 33 (if DEM < 1,000)
Herbaceous Tundra	20	
Wooded Tundra	21	
Mixed Tundra	22	
Bare Ground Tundra	23	66 (if DEM ≥ 3,400)
Snow or Ice	24	44

S2. MODIS Albedo Product (MCD43A4)

The MODIS Bidirectional Distribution Reflectance Model (BRDF) 16-Day surface albedo standard product (MCD43) has been validated though comparisons with in situ measurements [*Cescatti, Marcolla et al.*, 2012; *Stroeve, Box et al.*, 2013]. The high-quality primary algorithm MCD43 has also been shown to produce consistent global quantities over a variety of land surface types and snow-covered conditions [*Román, Gatebe et al.*, 2013]. The MCD43 is available globally from 2000 at resolutions of 0.5 to 5 km. We used the nadir BRDF-adjusted reflectance MCD43A4 (MODIS Terra + Aqua Nadir BRDF-Adjusted Reflectance 16-Day L3 Global 500-m SIN Grid V005), which is computed for each MODIS spectral band (1-7) at the mean solar zenith angle. Two MCD43A4 images with strip numbers of h23v04 and h24v04 on July 3, 2012 were downloaded from https://modis.gsfc.nasa.gov/data. We reprocessed them using the same coordinate systems and resolutions via numerical simulations.

S3. MODIS LAI Product (MYD15A2)

The MODIS global LAI product has been validated using Committee on Earth Observation Satellites (CEOS) Stage 2 data [*Yan, Park et al.*, 2016a; *Yan, Park et al.*, 2016b] and has been determined to have strong continuity and consistency for all biome types. On global and regional scales, earth observation (EO)-based estimates of LAI serve as valuable inputs for climate and hydrologic modeling [*Fensholt, Sandholt et al.*, 2004]. In this study, the level-4 MODIS global LAI MYD15A2 (MODIS/Terra+Aqua LAI/FPAR 8-Day L3 Global 1-km SIN Grid V005) was used. The data were downloaded from the website listed in section 2.2.3 and reprocessed using the same coordinate system and resolution as in the numerical simulation.

S4. GVF Data from MODIS Vegetation Indices (VI) (MOD13A2)

Currently, the MODIS VI product suite is now applied frequently in ecosystem, climate, and natural resources management studies and operational research. Stage 3 validation has been achieved for the MODIS VI (MOD13) [*Sesnie, Dickson et al.*, 2012; *Sims, Rahman et al.*, 2011]. Analyses produced by various airborne and field validation campaigns demonstrate that over most biomes, MODIS near-nadir satellite VI shows strong agreement with top-of-canopy nadir VI and land surface biophysical properties. The accuracy of the Normalized Difference Vegetation Index (NDVI) is within ± 0.025, and on a good-quality day (high quality without the nadir view requirement), it is within ±0.020. Using the qualified MODIS NDVI, the GVF can be calculated as follow [*Miller, Barlage et al.*, 2006; *Seungbum, Lakshmi et al.*, 2009; *Yin, Zhan et al.*, 2016]:

$$\mathrm{GVF} = \frac{\mathrm{NDVI} - \mathrm{NDVI_S}}{\mathrm{NDVI_V} - \mathrm{NDVI_S}} \quad (1)$$

where NDVI represents the NDVI value for each pixel from the MODIS NDVI product, $\mathrm{NDVI_S}$ represents the NDVI value for a sparsely vegetated or barren vegetation area, and $\mathrm{NDVI_V}$ represents the NDVI value corresponding to a fully vegetated area. Both $\mathrm{NDVI_V}$ and $\mathrm{NDVI_S}$ are constant, allowing the pixel-level GVF to reach theoretical values of 0.0 to 1.0 for any LU. In reference to previous paper [*Gutman and Ignatov*, 1998; *Jiang, Kogan et al.*, 2010; *Li and Zhang*, 2016; *Zeng, Dickinson et al.*, 2000], $\mathrm{NDVI_S}$ and $\mathrm{NDVI_V}$ were empirically determined to be 0.05 and 0.87, respectively. These

two parameters serve as global bounds to ensure that the derived GVFs vary from 0.0 to 1.0 (i.e., GVF = 1.0 when NDVI > 0.87 and GVF = 0.0 when NDVI < 0.05 in Equation 1). The MOD13A2 [*Didan*, 2015] Version 6 product (MODIS/Terra VI 16-Day L3 Global 1-km Grid SIN V006) was downloaded from https://lpdaac.usgs.gov/dataset_discovery and reprocessed using same coordinate system and resolution as in the simulations.

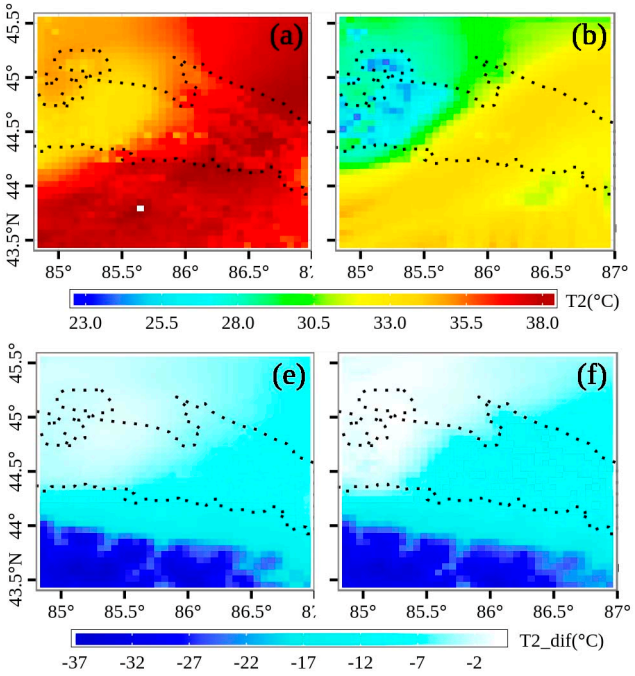

Figure S1. Mean 2-m air temperatures (T2) from the (**a,b**) *non-mountain* simulation, and (**c,d**) differences between *mod* and *non-mountain* simulations during daytime and nighttime, respectively.

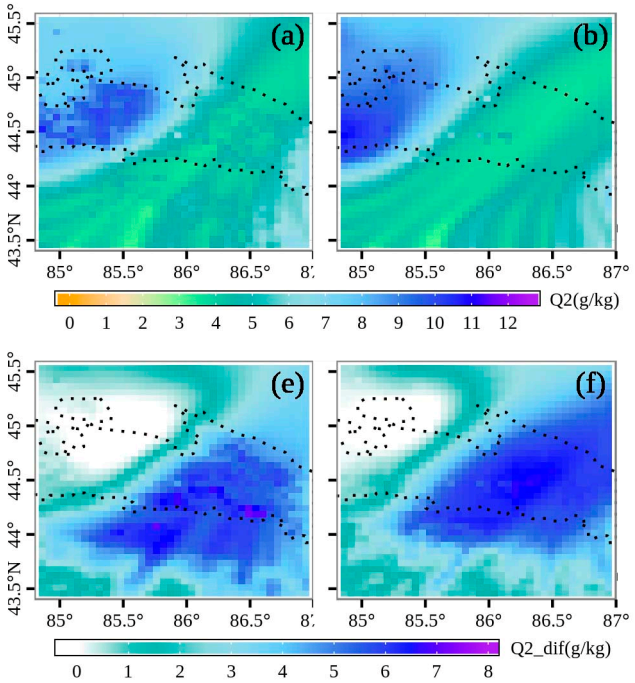

Figure S2. As Figure S1 but for surface specific humilities Q2 (g kg^{-1}).

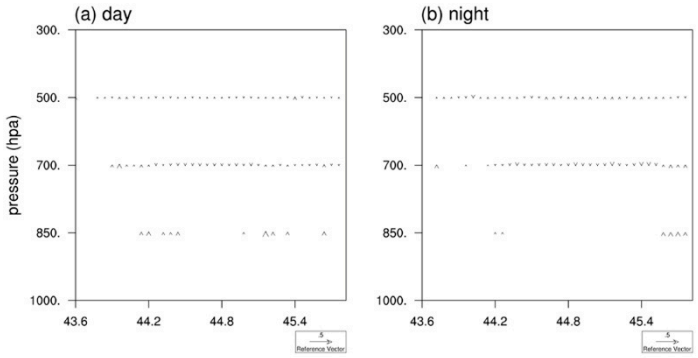

Figure S3. The W component difference between the *mod* simulation and *non-oasis* simulation during (a) daytime and (b) nighttime.

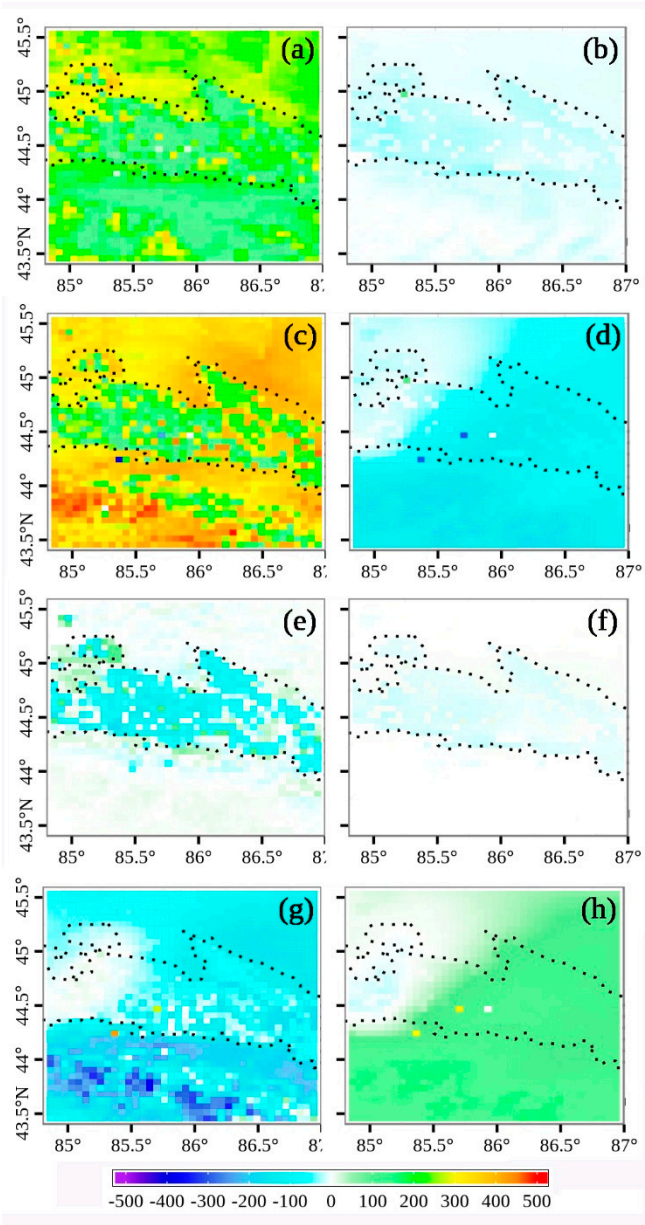

Figure S4. The mean sensible heat flux from the (**a, b**) *mod* simulation nd (**c,d**) *non-mountain* simulation during daytime and nighttime, and (**e, f**) differences between *mod* and *non-oasis* simulations and (**g,**

h) differences between *mod* and *non-mountain* simulations. The black dotted line represents the oasis border.

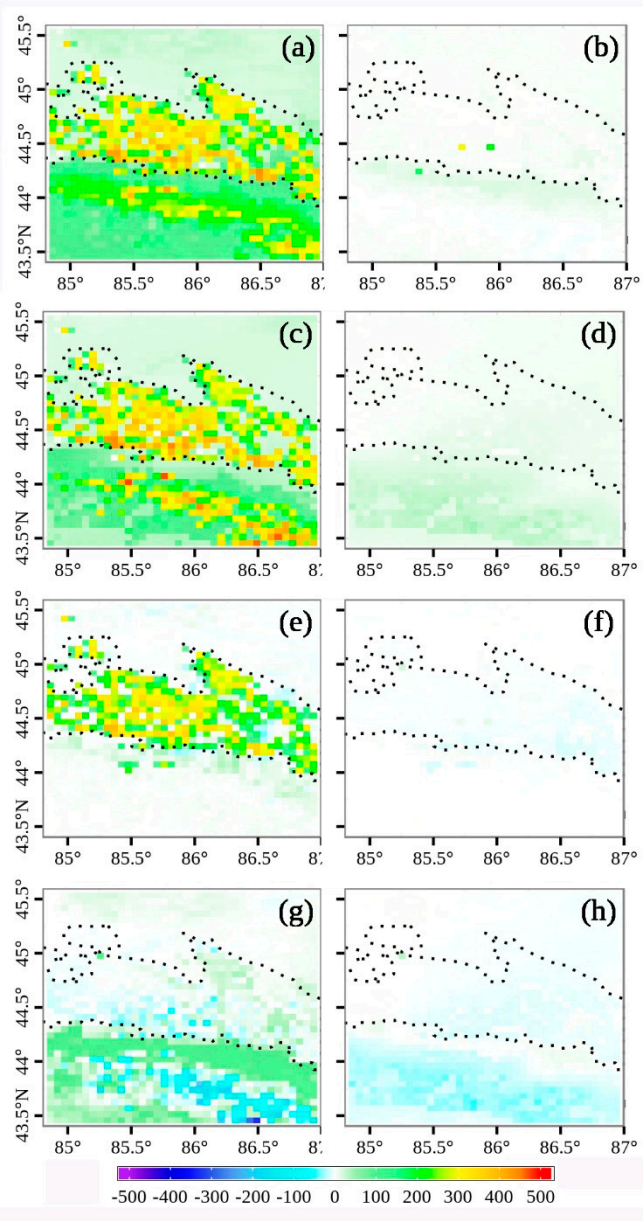

Figure S5. As Figure S4, but for mean Latent heat flux.